ISSN 0036-0244, Russian Journal of Physical Chemistry A, 2020, Vol. 94, No. 6, pp. 1254–1261. © Pleiades Publishing, Ltd., 2020.

PHOTOCHEMISTRY AND MAGNETOCHEMISTRY

Synthesis of $Bi/Bi_2O_2SiO_3/Bi_2WO_6$ Composites with Enhanced Visible Light Activity in Photocatalytic Degradation of Organic Compounds

Zhi Zhang[a], Chentao Zou[a], Jian Zhou[a], Zhiyuan Yang[a], Mengjun Liang[a], Min Wu[a], and Shuijin Yang[a,*]

[a]*College of Chemistry and Chemical Engineering, Hubei Key Laboratory of Pollutant Analysis and Reuse Technology, Hubei Normal University, Huangshi, Hubei, 435002 China*

**e-mail: yangshuijin@hbnu.edu.cn*

Received July 19, 2019; revised November 5, 2019; accepted November 12, 2019

Abstract—$Bi/Bi_2O_2SiO_3/Bi_2WO_6$ composite photocatalysts were synthesized via a simple reduction method with using ethylene glycol (EG) as reducing agent. Compared to the pure semiconductor, $Bi/Bi_2O_2SiO_3/Bi_2WO_6$ showed the highest photoactivity in degradation of rhodamine B (RhB) and ciprofloxacin (CIP) under visible light. The enhanced phtocatalytic performance can be primarily attributed to the improved visible light absorption and the effective separation of the charge carries by introducing $Bi_2O_2SiO_3$ and Bi produced surface plasmon resonance (SPR) effect, which is confirmed by UV–Vis diffuse refectance spectroscopy (DRS) and the photoelectrochemical measurements. In addition, cycle experiments explored the reliable stability and reusability for catalyst. Moreover, radical species trapping experiments demonstrated that holes (h^+) played crucial role in photodegradation process. This study may help promote the development of eliminate organic pollutants and environmental protection.

Keywords: metallic Bi, SPR effect, $Bi/Bi_2O_2SiO_3/Bi_2WO_6$ composites, photodegradation

DOI: 10.1134/S0036024420060369

INTRODUCTION

Recently, photocatalysts based on semiconductors received great attention as promising materials for environmental purification and solar energy utilization [1–3]. In various semiconductor photocatalysis, much attention has been given to Bi-based photocatalysts [4, 5]. As a visible-light response photocatalyst, Bi_2WO_6 possesses many advantages such as unique layered structure, stable properties and so on [6, 7], but it still need further improvements due to the low charge separation efficiency [8, 9].

To date, a lot of Bi-based heterojunction with Bi_2WO_6 enhanced visible light-driven photocatalysts were reported, such as Bi_2S_3/Bi_2WO_6 [10], $Bi_2WO_6/BiOBr$ [11], $Bi_2Fe_4O_9/Bi_2WO_6$ [12], and $BiVO_4/Bi_2WO_6$ [13]. Yang et al. [14] fabricated a composite of Bi_2WO_6 and BiOCl with a high activity in photodegradation of RhB, which is attributed to $Bi_2WO_6/BiOCl$ heterojunctions suppressing the recombination of the photoinduced electron–hole pairs. Therefore, it provides an idea that designing a composite photocatalyst by connecting Bi_2WO_6 with other semiconductors could be used to enhance the photocatalytic performance, but the molten salt method will cause larger expenses. $Bi_2O_2SiO_3$, as a highly active ultraviolent photocatalyst, has attracted more attention recently [15–17]. However, $Bi_2O_2SiO_3$ can only be applied in the ultraviolet region because of the wide bandgap (~3.5 eV) [18, 19], it is necessary to take effective measures to expand the photo-response range of $Bi_2O_2SiO_3$. Lu et al. [20] prepared $Bi_2O_3/Bi_2O_2SiO_3$ heterojunction with enhanced photocatalytic performance. The reported system was prepared by a facile one-step calcination method. However, Bi_2O_3 at high temperatures is prone to crystal phase transition. Therefore, the narrow energy band of Bi_2O_3 is similar to Bi_2WO_6, and wide energy band of BiOCl is similar to $Bi_2O_2SiO_3$, we can consider fabricating $Bi_2O_2SiO_3/Bi_2WO_6$ composites due to the matchable energy levels and lattices.

In addition, the incorporation of noble metals (Ag, Au, Pt, et al.) onto Bi_2WO_6 could also expanded the light response range and promote the effective separation of photogenerated charge owing to the SPR effect [21, 22]. Unfortunately, these metals are expensive and not easy to collect. Recently, scientists found that metallic Bi also show the SPR effect which is similar to those of precious metals, and attracted extensive attention owing to its especial properties including narrow band gap, high carrier motility, and low effective mass [23–25]. In previous reports, $Bi/BiPO_4$ was prepared by using $NaBH_4$ as reducting agent to pro-

duce Bi [26]. This method is feasible but the reaction is too intense. Compared to other reducer (KBH_4, $NaBH_4$, or ethylene diamine), ethylene glycol (EG) is a mild reagent. Huang et al. [27] used EG to reduce Bi^{3+} to metallic Bi and fabricated Bi/Bi_2WO_6 heterojunction that exhibited improved photocatalytic activity.

Herein, based on merits and shortcomings of $Bi_2O_2SiO_3$ and Bi_2WO_6 photocatalysts, $Bi_2O_2SiO_3/Bi_2WO_6$ composites were prepared by hydrothermal method, and then, metallic Bi was deposited on the surfaces of the $Bi_2O_2SiO_3/Bi_2WO_6$ structure by EG reduction due to mild reducibility. And $Bi/Bi_2O_2SiO_3/Bi_2WO_6$ composites exhibited the improved activity in photodegradation of RhB and CIP under visible light. The chemical properties and the photocatalysis mechanism of $Bi/Bi_2O_2SiO_3/Bi_2WO_6$ were also investigated. It is postulated that the enhanced photocatalytic activity of $Bi/Bi_2O_2SiO_3/Bi_2WO_6$ composites should be attributed to the introduction of $Bi_2O_2SiO_3$ and Bi.

EXPERIMENTAL

Synthesis of the $Bi_2O_2SiO_3/Bi_2WO_6$ Photocatalysts

The preparation of $Bi_2O_2SiO_3$ was reported in [24]. For the preparation of $Bi_2O_2SiO_3/Bi_2WO_6$ composites, 0.2425 g $Bi(NO_3)_3 \cdot 5H_2O$ was dissolved in aqueous solution of nitric acid. Meanwhile, 0.0824 g $Na_2WO_4 \cdot 2H_2O$ was dissolved in 10 mL distilled water under constant stirring. Afterward, the Na_2WO_4 aqueous solution was added to $Bi(NO_3)_3$ solution slowly, and stirred for 0.5 h. Then, 0.0346 g $Bi_2O_2SiO_3$ powders were added to the mixture and stirred further. Finally, the precursor solution was transferred into a 45 mL Teflon-lined autoclave, heated at 160°C for 24 h. The precipitates were washed with deionized water and ethanol for several times, and dried at 80°C. The sample denoted as SW-20 when the mass ratio of $Bi_2O_2SiO_3/Bi_2WO_6$ was 0.2 : 1. According to different mass ratio, other samples were denoted as SW-10 and SW-25, respectively. Bi_2WO_6 was prepared by the same methods without $Bi_2O_2SiO_3$.

Synthesis of the $Bi/Bi_2O_2SiO_3/Bi_2WO_6$ Photocatalysts

$Bi/Bi_2O_2SiO_3/Bi_2WO_6$ heterostructure were prepared by using EG as solvent and reducing agent under solvothermal conditions. Typically, 0.01 g $Bi(NO_3)_3 \cdot 5H_2O$ was dispersed in 80 mL of EG solution. Then, 0.10 g $Bi_2O_2SiO_3/Bi_2WO_6$ composites (SW-20) sample was added into the above solution and stirred for 1 h. After that, the suspension was transferred into a 100 mL Teflon-lined stainless steel autoclave and kept at 180°C for 10 h. After cooling, the product was washed repeatedly by distilled water and ethanol, and dried at 80°C. By controlling the mass ratio of $Bi(NO_3)_3 \cdot 5H_2O$ and $Bi_2O_2SiO_3/Bi_2WO_6$ composites in the solution were 5, 10, and 15%, the corresponding samples were denoted as BSW-5, BSW-10, and BSW-15, respectively.

Characterization

The crystal phases of the samples were analyzed by X-ray diffraction (XRD, Rigaku Ultima). The surface morphology of the products were analyzed by a Quanta 400 F scanning electron microscopy (SEM). Transmission electron microscopy (TEM) and high-resolution transmission electron microscopy (HR-TEM) images of the samples were obtained on a HITACHI HT770 transmission electron microscope. Fourier transform infrared spectra (FT-IR) were recorded in KBr pellets with a Nicolet 5700 spectrometer. UV–Vis diffuse refectance spectra (DRS) were measured on a UV-2500 UV–Vis spectrophotometer (Shimadzu, Japan). The total organic carbon (TOC) was measured on a TOC analyzer (TOC-L CPN). The photocurrent and electrochemical impedance spectra (EIS) of the samples were measured out on an electrochemical workstation (CHI 660).

Photocatalytic Activity Measurements

The as-prepared catalyst (20 mg) was added into 50 mL of RhB or CIP aqueous solution (both 10 mg/L) in quartz photochemical reactor and stirred in dark to establish the adsorption equilibrium. Then, the solution was irradiated with a 300 W Xe lamp with a cutoff filter ($\lambda \geq 420$ nm). The reaction mixture was periodically sampled; the samples were centrifuged, extracted and analyzed using UV–Vis spectrophotometer (UV-3010, Hitachi). The degradation efficiency was calculated as follows:

$$\eta = (C_0 - C)/C_0 \times 100\%,$$

where C_0 is the absorbance of original RhB or CIP solution and C is the absorbance of the RhB or CIP solution after irradiation. The photocatalytic process could be expressed as the following equation:

$$\ln(C_0/C) = kt,$$

where k is the apparent pseudo-first-order rate constant. Moreover, the recycling experiments were performed for five recycles to test the durability. After each cycle, the photocatalyst was centrifuged and used directly for the next test.

RESULTS AND DISCUSSION

XRD Analysis

The phase composition of the as-prepared samples was determined by XRD. As shown in Fig. 1, the diffraction peaks of pure Bi_2WO_6 at $2\theta = 28.3°$, 32.9°, 47.2°, 56.0°, and 58.5°, were assigned to the (131), (002), (202), (133), and (262) reflection of Bi_2WO_6

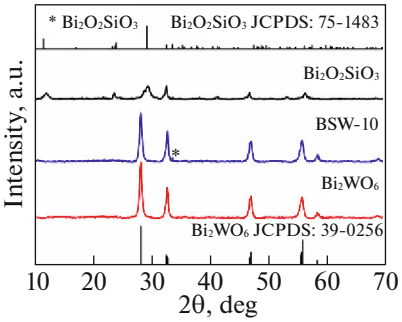

Fig. 1. (Color online) XRD pattern of as-synthesized samples.

(JCPDS no. 39-0256), respectively. Sharp and intense peaks indicate very high crystallinity [28]. For $Bi_2O_2SiO_3$, all diffraction peaks could be matched with the orthorhombic phase of $Bi_2O_2SiO_3$ (JCPDS no. 75-1483) [29]. As for the Bi/$Bi_2O_2SiO_3$/ Bi_2WO_6 composites (BSW-10), the weak diffraction peaks at 33.71° was observed, which can be assigned to (002) crystal phases of $Bi_2O_2SiO_3$ (JCPDS no. 75-1483). Moreover, there is no diffraction peaks for Bi in the composites of BSW-10, which might be due to the weak reducing ability of EG and higher dispersion of composites [30, 31].

XPS Analysis

The XPS survey spectra in Fig. 2a shows the presence of Bi, Si, W, O, C (C comes from reference sample) in BSW-10. Figure 2b features the two strong peaks centered at 164.1 and 158.8 eV are assigned to Bi $4f_{5/2}$ and Bi $4f_{7/2}$, respectively, which are the features of Bi^{3+} species of Bi_2WO_6 [27, 32]. Additionally, the shoulder bands with weak located at 161.8 and 156.6 eV confirms the generation of metallic Bi. As is shown in Fig. 2c, the two peaks at 37.2 and 35.0 eV are assigned to W $4f_{5/2}$ and W $4f_{7/2}$, which are feature of $[WO_4]^{2-}$ [33, 34]. The O 1*s* profiles in Fig. 2d can be fitted into three peaks, positioned at 529.5, 530.3 and 531.1 eV. The sub-band centered at 529.5 eV is characteristic of lattice oxygen species, such as $[Bi_2O_2]^{2+}$ and $[WO_4]^{2-}$ layers, and other two peaks around 530.3 and 531.1 eV are assigned to the hydroxyl-like group and the chemically adsorbed water, respectively [35].

SEM and TEM Analysis

The morphology of the as-prepared samples was characterized by SEM and TEM. Figure 3a shows that the pure $Bi_2O_2SiO_3$ has rod-like structure with the length of rods are 5–10 μm. As shown in Fig. 3b, Bi_2WO_6 sample consists of flower-like microspheres (~4 μm) self-assembled in nanosheets. It should be noted that the morphology of the BSW-10 composite is similar to that of pure $Bi_2O_2SiO_3$, with the Bi_2WO_6 nanosheets focus on the surface of $Bi_2O_2SiO_3$ rod-like structure and the length of BSW-10 composites about 20 μm (Fig. 3c). To further confirm the composition of composite, the BSW-10 sample was analyzed by TEM and HRTEM. As can be seen from Fig. 4a, there are some irregular spheres on the surface and spheres diameter is about 10–15 nm, which may be metal Bi. Figure 4b shows HRTEM image of BSW-10. By measuring the lattice fringes, the interplanar distance of 0.2717 and 0.3179 nm, which correspond to the (002) and (131) crystal plane of Bi_2WO_6, respectively.

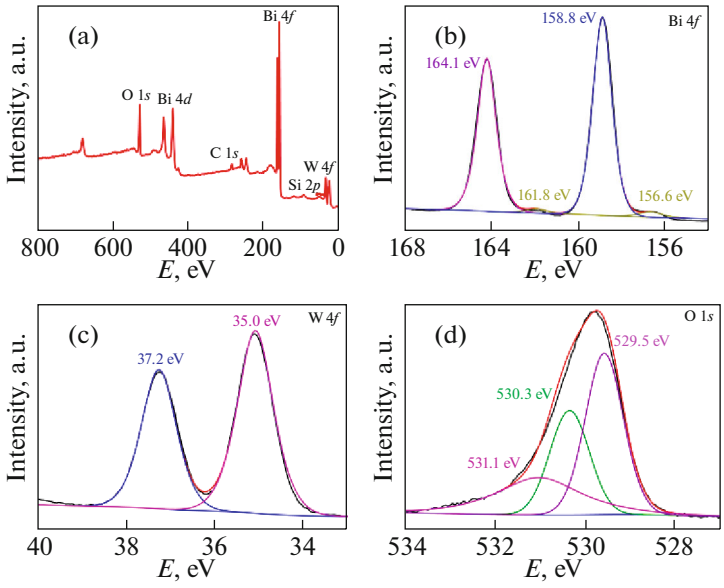

Fig. 2. (Color online) XPS spectra of sample BSW-10: survey (a), Bi 4*f* (b), W 4*f* (c), O 1*s* (d), *E* is binding energy.

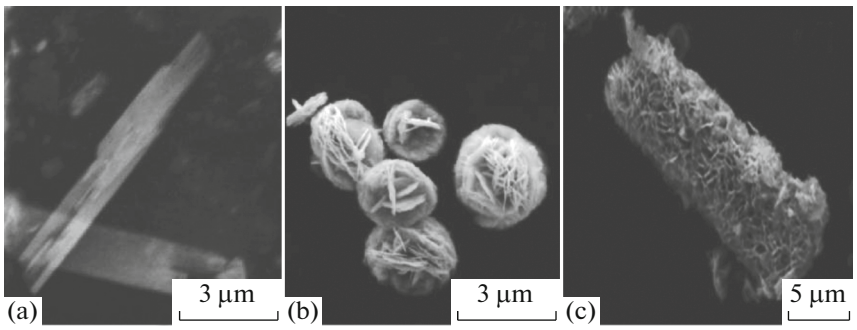

Fig. 3. SEM images of pure $Bi_2O_2SiO_3$ (a), Bi_2WO_6 (b), and BSW-10 (c).

The resolved interplanar distances of 0.2656 and 0.2894 nm are corresponding to (002) plane of $Bi_2O_2SiO_3$ and (211) plane of Bi (JCPDS no. 51-0765). These results further indicate that the successful fabrication of $Bi/Bi_2O_2SiO_3/Bi_2WO_6$ heterojunction, which are consistent with XRD and XPS data.

UV–Vis DRS Spectra

The optical absorption properties of the prepared material were evaluated by DRS (Fig. 5). Compared to $Bi_2O_2SiO_3$ and Bi_2WO_6, the composites of BSW-10 showed enhanced visible light absorption (Fig. 5a). Figure 5b shows the plot of $(\alpha h\nu)^{2/n}$ vs. $h\nu$ ($n = 4$ for $Bi_2O_2SiO_3$ and $n = 1$ for Bi_2WO_6), from which the band gap of the samples can be estimated, and the E_g of $Bi_2O_2SiO_3$, Bi_2WO_6, BSW-10 are 3.23, 2.90, and 2.83 eV, respectively. Obviously, the light absorption of the $Bi/Bi_2O_2SiO_3/Bi_2WO_6$ heterojunction is broadened the visible light range. The valence band (VB) and the conduction band (CB) potentials can be calculated by the empirical formula:

$$E_{VB} = X - E^e + 0.5E_g, \quad (1)$$

$$E_{CB} = E_{VB} - E_g, \quad (2)$$

where X is the absolute electronegativity of the semiconductor, being 6.474 and 5.55 eV for $Bi_2O_2SiO_3$ and Bi_2WO_6, respectively [36, 37], E_{VB} and E_{CB} are the VB and CB potentials, respectively, and E^e is the energy of free electrons on the hydrogen scale (4.5 eV vs. NHE). The E_{VB} and E_{CB} of $Bi_2O_2SiO_3$ were calculated to be 3.62 and 0.39 eV, respectively. For Bi_2WO_6, the E_{VB} and E_{CB} are 2.5 and –0.4 eV, respectively.

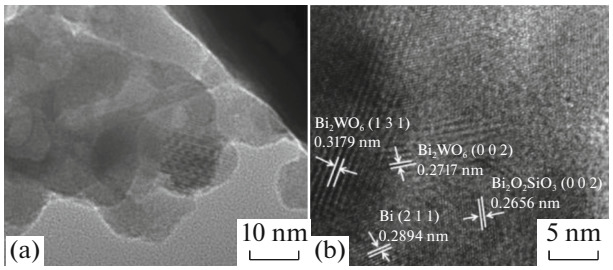

Fig. 4. TEM (a) and HRTEM (b) images of the sample BSW-10.

Photocatalytic Activity

In order to study the photocatalytic performance of the samples, the experiments on the photodegradation of RhB as well as CIP were carried out under visible light irradiation. First, compounding $Bi_2O_2SiO_3$ with Bi_2WO_6, the photocatalytic activity of RhB on the $Bi_2O_2SiO_3/Bi_2WO_6$ composites is shown in Fig. 6a. When the mass ratio of $Bi_2O_2SiO_3$ reaches 20%, the SW-20 sample's degradation efficiency of RhB is up to 83.3% under visible light irradiation after 40 min. After the introduction of Bi, BSW-10 sample shows highest activity under visible light irradiation degradation of 93.4% for 40 min. To have a better understanding of the reaction rate, the corresponding first-order kinetics plots were fitted and shown in Fig. 6b [38]. The accuracy of k and R^2 parameter were given in Table 1. It is seen that the kinetic plots of the RhB degradation exhibit good linear variation with irradiation time, and the correlation coefficients for the regression lines is larger than 0.9 (i.e., $R^2 > 0.9$).

It is well known that the mineralization is the final goal in pollutant treatment, and TOC value is usually used as an important index for the mineralization of organic species. The mineralization of RhB was investigated by loading 20 mg catalysts in 50 mL RhB aqueous solution (10 mg L^{-1}) under visible-light irradiation, and TOC value at before and after reaction was recorded. The TOC removal was shown in Fig. 6c, in which the red color marked as the initial TOC value of RhB, and the gray part marked as TOC value after 40 min irradiation. Obviously, with the BSW-10 sample, the final TOC concentration is minimum. This result demonstrates that $Bi/Bi_2O_2SiO_3/Bi_2WO_6$ structures can efficiently degrade and mineralize organic pollutants under visible-light irradiation.

To eliminate the photosensitization in the RhB photocatalytic decomposition process, colorless CIP

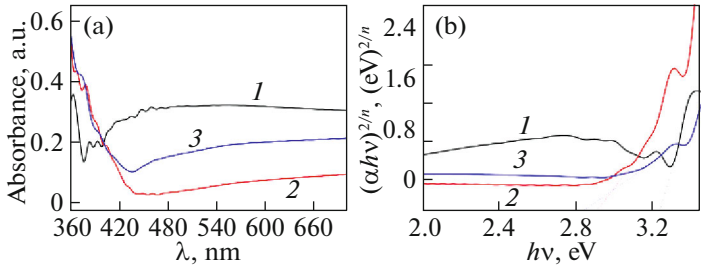

Fig. 5. (Color online) The UV–Vis diffuse reflectance spectra (a) and the plots of $(\alpha h\nu)^{2/n}$ vs. photon energy ($h\nu$) for the band-gap energies of samples (b); *1*–$Bi_2O_2SiO_3$, *2*–Bi_2WO_6, *3*–BSW-10.

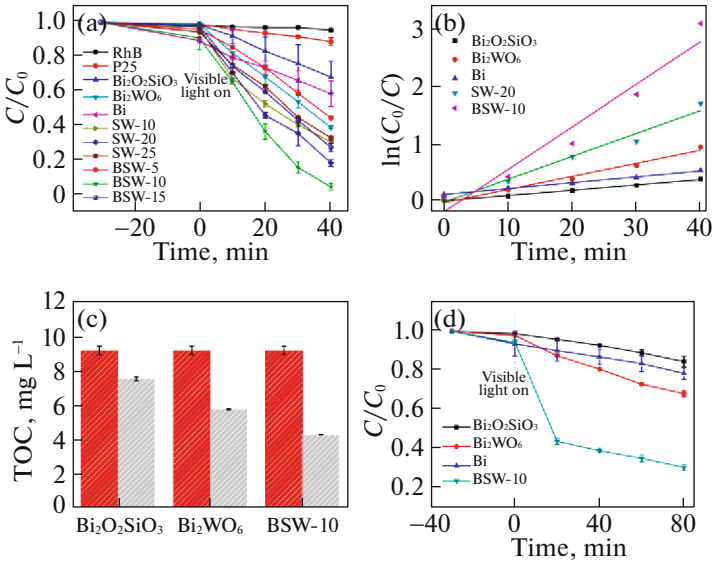

Fig. 6. (Color online) Photocatalytic degradation efficiencies of RhB over different samples (a), first-order kinetics plots for the photocatalytic degradation of RhB under the irradiation of visible light (b), the TOC removal efficiency over different catalysts (c), and photocatalytic degradation efficiencies of CIP under visible light irradiation (d).

was selected as a model pollutant, as shown in Fig. 6d. This result is similar to the degradation of RhB solution, BSW-10 has the highest photocatalytic activity, the degradation rate of CIP is 69% after visible light irradiation for 80 min.

The stability of $Bi/Bi_2O_2SiO_3/Bi_2WO_6$ composites was also studied through the degradation of RhB under visible light irradiation. As displayed in Fig. 7a, after five cycles, the BSW-10 sample still remains high photocatalytic performance and the photocatalytic activity of degradation of RhB is 87.36%, which indicates the $Bi/Bi_2O_2SiO_3/Bi_2WO_6$ composites have high stability and reusability in the photocatalytic reaction. Figure 7b shows the FT-IR pattern before and after cycles of BSW-10. The weak peaks located around 1029 cm^{-1} was decline due to the low content of $Bi_2O_2SiO_3$ and there is no obvious change in other places, confirming the recyclability of the BSW-10 catalyst.

Photocatalytic Mechanism Analysis

The separation of charges makes a difference in the photodegradation process which can be measured by EIS and the photocurrent. A higher mobility of photo-excited carriers will cause smaller EIS arc radius. Furthermore, higher photocurrent intensity means more electron-hole pairs are generated [39, 40]. As shown in Fig. 8a, the diameter of Nyquist circle of BSW-10 features is smallest radius among all samples, demonstrating the fastest charge transfer property of BSW-

Table 1. The k value and fitting coefficient R^2 in photocatalytic degradation of RhB on the samples

Value	Bi	$Bi_2O_2SiO_3$	Bi_2WO_6	SW-20	BSW-10
k, min^{-1}	0.0133	0.0095	0.0235	0.0424	0.0773
R^2	0.99289	0.99197	0.97754	0.96726	0.92788

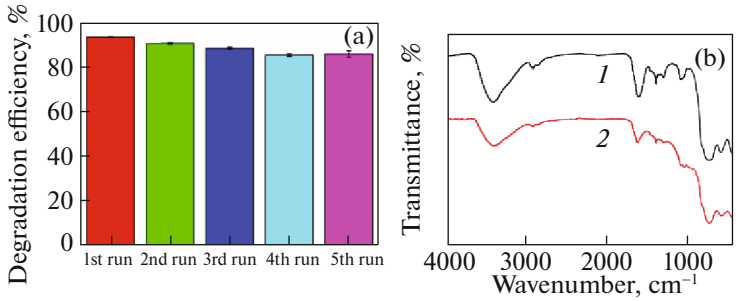

Fig. 7. (Color online) Cycling performance of BSW-10 for the degradation of RhB under visible light irradiation (a) and FT-IR patterns at before (*1*) and after (*2*) cycle experiments (b).

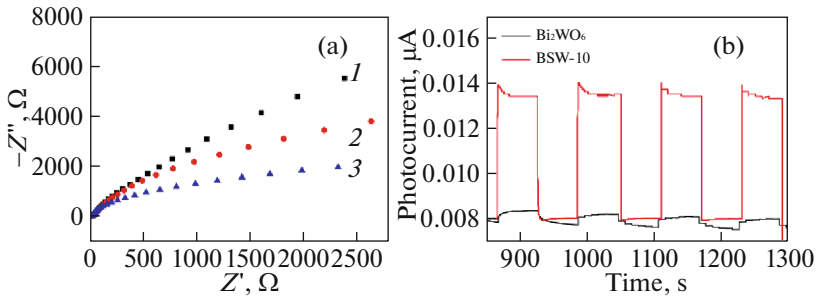

Fig. 8. (Color online) The EIS spectra (a) and photocurrent responses (b) of samples; *1*—$Bi_2O_2SiO_3$, *2*—Bi_2WO_6, *3*—BSW-10.

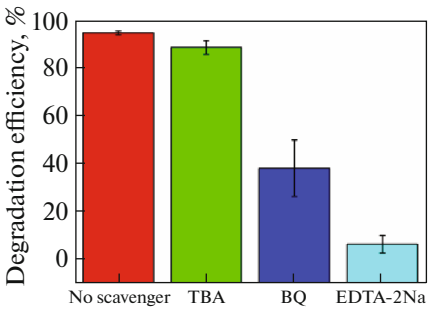

Fig. 9. (Color online) The active species trapping experiment of BSW-10 for the degradation of RhB.

10. From Fig. 8b, BSW-10 exhibited the higher photocurrent density in comparison with Bi_2WO_6, which indicates that BSW-10 generates more electron-hole pairs with excellent separation efficiency under visible light.

It is important to detect the main reactive species in the photocatalytic process to reveal the photocatalytic mechanism. Benzoquinone (BQ), ethylenediaminetetraacetic acid disodium salt (EDTA-2Na), and *tert*-butanol (TBA) were added to act as the scavengers for superoxide radical ($^{\bullet}O_2^-$), holes (h^+), and hydroxyl radical ($^{\bullet}OH$), respectively. As shown in Fig. 9, under the visible light irradiation of the BSW-10 sample, the degradation efficiency of RhB is significantly inhibited by adding EDTA-2Na and BQ scavengers, implying that h^+ and $^{\bullet}O_2^-$ radicals play major roles in the catalytic processes and the addition of TBA shows a weaker influence on the photocatalytic degradation. In the presence of BQ, there was large fluctuation, which may attributed to the adsorption of BQ. This result clearly demonstrates that h^+ plays more vital roles than $^{\bullet}O_2^-$ and $^{\bullet}OH$ in the photodegradation process of RhB over BSW-10 sample.

According to the above systematic analysis, a mechanism for the improved photocatalytic activity of $Bi/Bi_2O_2SiO_3/Bi_2WO_6$ is proposed, as illustrated in Fig. 10. According to literature [27], the Fermi level (vs. NHE) of Bi can be estimated to be about −0.17 eV and the CB potential of Bi_2WO_6 is −0.4 eV. Comparing with the Fermi level of metal Bi, the CB of Bi_2WO_6 is more negative. Due to excellent chemical properties, Bi_2WO_6 could be excited under visible light irradiation to the photogenerated electrons in the CB and holes in the VB, respectively. Then, the electrons could transfer from CB of Bi_2WO_6 to Bi metal. Furthermore, the Fermi level of Bi is higher than the CB of $Bi_2O_2SiO_3$ (+0.39 eV), and the photogenerated electrons in Bi were therefore transferred to $Bi_2O_2SiO_3$. Compared with the standard redox potential of $^{\bullet}OH/H_2O$ (+2.8 eV) [41, 42] the VB of Bi_2WO_6 is not positive enough to generate $^{\bullet}OH$. Due to the redox potential of $O_2/^{\bullet}O_2^-$ (−0.33 eV) [43] is more positive than the CB of

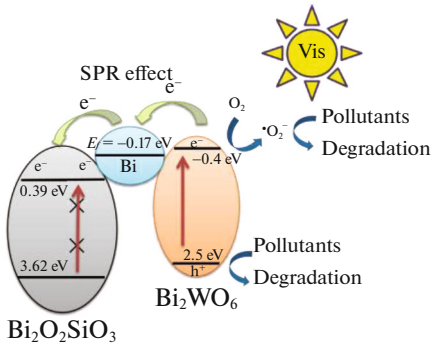

Fig. 10. (Color online) The mechanism of the photocatalytic reaction over the $Bi/Bi_2O_2SiO_3/Bi_2WO_6$ system.

Bi_2WO_6, the separated electrons will react with the O_2 and reduce it to $^{\bullet}O_2^-$. Finally, h^+ and $^{\bullet}O_2^-$ degrade pollutants. Therefore, the enhanced photocatalytic performance was ascribed to the formation of $Bi/Bi_2O_2SiO_3/Bi_2WO_6$ heterojunction improving the separation of electron-hole pairs.

CONCLUSIONS

In summary, $Bi/Bi_2O_2SiO_3/Bi_2WO_6$ composites photocatalyst was prepared by reduction with EG. The photocatalytic activity of $Bi/Bi_2O_2SiO_3/Bi_2WO_6$ is evaluated by the photodegradation of RhB and CIP under visible light irradiation. The improved photocatalytic activity can be ascribed to the introduction of $Bi_2O_2SiO_3$ and the SPR effect of metallic Bi, where the SPR effect of the introduced Bi not only significantly enhances the light absorption, but also leads to efficient separation and transferring of photogenerated charge carriers. This study confirms that connecting the narrow band gap with wide band gap semiconductors, and then, deposition of metallic Bi using EG as a reducing agent could provide a great idea for future photodegradation processes.

ACKNOWLEDGMENTS

This work was kindly supported by the National Natural Science Foundation of China (21171053), Hubei Province Undergraduate Training Programs for Innovation and Entrepreneurship (201810513073), Graduate Student Innovation Research Foundation of Hubei Normal University (2018039) and Institute for Advanced Materials of Hubei Normal University.

REFERENCES

1. R. Moradi, M. Hamidvand, and A. Ganjali, Russ. J. Phys. Chem. A **93**, 1133 (2019).
2. Y. Huang, K. Yao, M, Xiang, M. Jia, and A. Zhang, Russ. J. Phys. Chem. A **93**, 1182 (2019).
3. Y. Chen, J. Li, and Y. Liang, Russ. J. Phys. Chem. A **93**, 1406 (2019).
4. C. Zou, Z. Yang, M. Liang, Y. He, Y Yun, and S. Yang, Nano **13**, 1850070 (2018).
5. S. Zhu, C. Yang, F. Li, T. Li, M. Zhang, and W. Cao, Mol. Catal. **435**, 33 (2017).
6. Z. Yang, L. Chen, Y. Yang, J. Wang, Y. Huang, X. Liu, and S. Yang, Semicond. Sci. Technol. **32**, 065008 (2017).
7. X. Xiao, J. Wei, Y. Yang, R. Xiong, C. Pan, and J. Shi, ACS Sustainable Chem. Eng. **4**, 3017 (2016).
8. L. Yao, W. Wang, Y. Liang, J. Fu, and H. Shi, Appl. Surf. Sci. **469**, 829 (2019).
9. Y. Zhu, Y. Wang, Q. Ling, and Y. Zhu, Appl. Catal., B **200**, 222 (2017).
10. F. Xu, C. Xu, H. Chen, D. Wu, Z. Gao, X. Ma, Q. Zhang, and K. Jiang, J. Alloys Compd. **780**, 634 (2019).
11. X. Ren, K. Wu, Z. Qin, X. Zhao, and H. Yang, J. Alloys Compd. **788**, 102 (2019).
12. B. Li, C. Lai, G. Zeng, L. Qin, H. Yi, D. Huang, C. Zhou, X. Liu, M. Cheng, P. Xu, F. Huang, and S. Liu, ACS Appl. Mater. Interfaces **10**, 18824 (2018).
13. L. Ji, L. Lin, D. Yu, P. Gao, and B. Liu, Mater. Lett. **220**, 94 (2018).
14. Q. Yang, M. Luo, K. Liu, H. Cao, and H. Yan, Chem. Commun. **55**, 5728 (2019).
15. D. Liu, W. Yao, J. Wang, Y. Liu, M. Zhang, and Y. Zhu, Appl. Catal., B **172**, 100 (2015).
16. D. Liu, J. Wang, M. Zhang, Y. Liu, and Y. Zhu, Nanoscale **6**, 15222 (2014).
17. D. Liu, W. Cai, Y. Wang, and Y. Zhu, Appl. Catal., B **236**, 205 (2018).
18. Z. Wan, and G. Zhang, J. Mater. Chem. A **3**, 16737 (2015).
19. C. Yang, W. Lee, H. Lin, Y. Dai, H. Chi, and C. Chen, RSC Adv. **6**, 40664 (2016).
20. H. Lu, Q. Hao, T. Chen, L. Zhang, D. Chen, C. Ma, W. Yao, and Y. Zhu, Appl. Catal., B **237**, 59 (2018).
21. X. Hu, J. Tian, Y. Xue, Y. Li, and H. Cui, ChemCatChem **9**, 1511 (2017).
22. J. Jia, X. Du, E. Liu, J. Wan, C. Pan, Y. Ma, X. Hu, and J. Fan, J. Phys. D: Appl. Phys. **50**, 145103 (2017).
23. F. Yang, X. Zhu, J. Fang, D. Chen, W. Feng, and Z. Fang, Ceram. Int. **44**, 6918 (2018).
24. X. Li, W. Zhang, J. Li, G. Jiang, Y. Zhou, S. Lee, and F. Dong, Appl. Catal., B **241**, 187 (2019).
25. S. Zhao, Z. Dai, W. Guo, F. Chen, Y. Liu, and R. Chen, Appl. Catal., B **244**, 206 (2019).
26. J. Li, W. Zhang, M. Ran, Y. Sun, H. Huang and F. Dong, Appl. Catal., B **243**, 313 (2019).
27. Y. Huang, S. Kang, Y. Yang, H. Qin, Z. Ni, S. Yang, and X. Li, Appl. Catal., B **196**, 89 (2016).
28. M. Arif, M. Zhang, Y. Luo, H. Yin, and X. Liu, J. Ind. Eng. Chem. **69**, 345 (2019).
29. J. Di, J. Xia, Y. Huang, M. Ji, W. Fan, Z. Chen, and H. Li, Chem. Eng. J. **302**, 334 (2016).
30. X. Liu, L. Pan, T. Lv, and Z. Sun, J. Collid Interface Sci. **394**, 441 (2013).

31. F. Tian, H. Zhao, G. Li, Z. Dai, Y. Liu, and R. Chen, ChemSusChem **9**, 1579 (2016).
32. D. Wang, L. Guo, Y. Zhen, L. Yue, G. Xue, and F. Fu, J. Mater. Chem. A **2**, 11716 (2014).
33. J. Yang, X. Wang, X. Zhao, J. Dai, and S. Mo, J. Phys. Chem. C **119**, 3068 (2015).
34. Y. Peng, M. Yan, Q. Chen, C. Fan, and H. Zhou, J. Mater. Chem. A **2**, 8517 (2014).
35. C. Wu, H. Chang, and J. Chern, J. Hazard. Mater. **137**, 336 (2006).
36. J. Liu, Y. Li, Z. Li, J. Ke, and H. Xiao, Catal. Today **314**, 2 (2018).
37. X. Liu, W. Wang, Y. Liu, B. Huang, Y. Dai, X. Qin, and X. Zhang, RSC Adv. **5**, 55957 (2015).
38. H. Dong, G. Chen, J. Sun, Y. Feng, C. Li, and G. Xiong, Dalton Trans. **43**, 7282 (2014).
39. C. Wang, X. Zhang, Y. Zhang, J. Chen, G. Huang, J. Jiang, W. Wang, and H. Yu, Appl. Catal., B **237**, 464 (2018).
40. S. Xiao, Y. Li, J. Hu, H. Li, X. Zhang, L. Liu, and J. Li-an, CrystEngComm **17**, 3809 (2015).
41. J. Wang, L. Tang, G. Zeng, Y. Liu, Y. Zhou, Y. Deng, J. Wang, and B. Peng, ACS Sustainable Chem. Eng. **5**, 1062 (2017).
42. S. Kumar, A. Baruah, S. Tonda, B. Kumar, V. Shanker, and B. Sreedhar, Nanoscale **6**, 4830 (2014).
43. S. Wang, X. Yang, X. Zhang, X. Ding, Z. Yang, K. Dai, and H. Chen, Appl. Surf. Sci. **391**, 194 (2017).